Bulletin of Earthquake Engineering
https://doi.org/10.1007/s10518-026-02443-7

ORIGINAL ARTICLE

# A new global vulnerability model for regional seismic risk assessments: Part 1 – structural vulnerability

**Karim Aljawhari**[1,2] · **Al Mouayed Bellah Nafeh**[1] · **Vitor Silva**[1,3]

Received: 24 October 2025 / Accepted: 16 March 2026
© The Author(s) 2026

**Abstract**
Reliable vulnerability functions are central to earthquake risk assessments. Yet many functions used in national, regional, and global contexts still rely on oversimplified numerical representations that cannot adequately capture the complex seismic behaviour of buildings, which can bias predictions of structural performance and earthquake-induced losses. As part of the new Global Vulnerability Model supported by the Global Earthquake Model (GEM) Foundation, we introduce a new, upgraded structural vulnerability database for large-scale seismic risk modelling. Compared to the previous version, the new database: (1) expands the number of building classes from 500 classes to nearly 1,000, capturing a wider range of structural systems and seismic design-code levels; (2) adopts an improved numerical modelling strategy based on efficient multi-degree-of-freedom *stick-and-mass* models to simulate seismic response at scale; (3) assembles an extensive suite of ground-motion records for response analysis spanning diverse tectonic environments (e.g., active shallow crust, stable continental, and subduction zones); and (4) develops a new set of fragility and vulnerability functions tailored to structural damage. Together, these advances provide a more robust basis for estimating damage and monetary losses within GEM's new Global Seismic Risk Model. All derived functions are released in an open-access repository to support both probabilistic and scenario-based seismic risk assessments.

**Keywords** Vulnerability · Fragility · Structural performance · Earthquake · Losses · Multi-degree-of-freedom · Seismic risk

✉ Karim Aljawhari
karim.aljawhari@globalquakemodel.org

[1] Global Earthquake Model (GEM) Foundation, Pavia, Italy

[2] Department of Civil, Environmental, and Geomatic Engineering, University College London (UCL), London, UK

[3] Department of Civil Engineering, University of Aveiro, Aveiro, Portugal

Published online: 05 June 2026

## 1 Introduction

Earthquakes remain among the most damaging natural hazards, with more than one million deaths and nearly a trillion USD in economic losses recorded over the past century (Sen 2009; Elnashai and Di Sarno 2015). A substantial share of these impacts stems from inadequate performance of buildings not designed to satisfy seismic codes/provisions (e.g., Bull 2013; So 2016; Gautam and Chaulagain 2016). This makes it essential to provide reliable vulnerability functions for producing meaningful economic loss estimates in seismic risk assessments, thereby shaping how risk drivers are identified and how priorities are set for mitigation and resilience planning. A holistic loss estimate must address the seismic performance of multiple building component types, including structural, non-structural, as well as contents. Structural response nevertheless remains the cornerstone of risk models, as it largely governs damage progression and collapse potential.

As part of the first Global Seismic Risk Model (Silva et al. 2020) developed by the Global Earthquake Model (GEM) Foundation in 2018, Martins and Silva (2021) introduced a large database of fragility and vulnerability functions. Fragility functions quantify the probability of exceeding a set of damage states (DSs), conditioned on a suitable ground-shaking intensity measure (IM). To estimate economic losses, these fragilities were combined with damage-to-loss ratios (e.g., Dolce et al. 2006; FEMA 2012a), which map each DS to an expected loss, expressed as a fraction of building replacement cost. This generates vulnerability functions defining the loss ratio across a range of IM levels (e.g., Martins et al. 2016; Aljawhari et al. 2024). The database covered about 500 building classes, modelled as simplified single-degree-of-freedom (SDOF) oscillators and analysed via nonlinear time-history analysis (NLTHA) to simulate their seismic performance.

The Martins and Silva (2021) database marked a key step toward globally available vulnerability functions; however, its reliance on SDOF oscillators and simplified modelling assumptions constitutes a major limitation. While SDOF models can represent the global behaviour of first-mode dominated structures, they fall short in capturing more complex mechanisms like inelastic demand concentration and higher-mode effects (e.g., Nettis et al. 2021; Suzuki and Iervolino 2021; Angelucci et al. 2022). As a result, they cannot provide storey-level seismic demand parameters in multi-storey buildings, such as peak storey drift (PSD) and peak floor acceleration (PFA), which are critical for damage and loss assessment, especially for non-structural components and building contents. Another limitation is the relatively limited set of ground-motion records used for the NLTHA.

To overcome these challenges, building-specific risk assessment approaches, such as FEMA P-58 (Günay and Mosalam 2013), have gained traction because they estimate losses at the component level, providing much greater fidelity in representing seismic damage and its consequences. Such approaches typically require refined multi-degree-of-freedom (MDOF) models capable of capturing inelastic mechanisms in individual building components, together with hazard-consistent ground-motion records and detailed inventories of component-level fragility and loss/consequence models. Although effective for single-building assessments, their computational demands make them impractical for large-scale regional applications.

To bridge the gap between the accuracy of detailed MDOF models and the efficiency of SDOF oscillators, particularly in regional studies, several researchers have advocated simplified mechanical MDOF representations like *fish-bone* models (e.g., Soleimani et al.

2019; Jamšek and Dolšek 2020) or *stick-and-mass* models (e.g., Xiong et al. 2016; Lu et al. 2018; Gaetani d'Aragona et al. 2020). These models simulate the shear response of individual storeys, allowing reliable estimation of interstorey seismic demands at a substantially reduced computational cost. Extensions to these models have also been proposed to address torsional response, masonry infill walls, and soil-structure interaction (Blasone et al. 2022, 2025; Angelucci et al. 2025).

Despite the above advancements, a comprehensive database of reliable MDOF models encompassing a broad range of building classes, along with refined fragility and vulnerability functions, is still lacking. To address this need, our study leverages the Martins and Silva (2021) database and delivers four major innovations: (1) expanding the covered building classes from 500 to approximately 1,000; (2) replacing the original SDOF oscillators with efficient *stick-and-mass* MDOF systems, enabling explicit evaluation of storey demands and more complex inelastic mechanisms; (3) compiling an extensive dataset of ground-motion records from diverse tectonic environments for use in NLTHA; and (4) deriving a new suite of structural fragility and vulnerability functions that provide more realistic predictions of seismic damage and loss across all building classes. The new database is compared against the original version, unveiling systematic differences that underscore the sensitivity of regional risk assessments to modelling assumptions.

This paper presents Part I of GEM's new Global Vulnerability Model, focusing on the numerical modelling strategy, analysis workflow, and derivation of structural fragility and vulnerability functions. A companion paper (Part II) (Nafeh et al. 2026b) extends this framework to seismic losses associated with non-structural components and building contents. Methodologically, Part I derives structural fragility and vulnerability through drift-based global DSs, whereas Part II estimates non-structural losses via region- and occupancy-specific storey loss functions, coupled with storey- and floor-level seismic demand profiles. The two parts are linked through the seismic performance assessment, as the NLTHA conducted in Part I provides the storey-drift and floor acceleration profiles required in Part II to quantify non-structural and content losses. Together, the fragility and vulnerability functions from Parts I and II facilitate damage and economic loss assessment within the 2026 version of the Global Seismic Risk Model, and they are publicly available in an open-access GitHub[1] repository.

## 2 New global vulnerability database: methodology

The methodology adopted to develop the new global vulnerability database is depicted in Fig. 1. The workflow begins with numerical modelling of *stick-and-mass* MDOF systems for about 1,000 building classes. The nonlinear dynamic behaviour of the models is assessed via a cloud-based NLTHA (Cornell et al. 2002; Jalayer et al. 2017), adopting a new extensive suite of ground motions. These analyses provide basis for deriving fragility functions characterising structural damage conditional on a ground-shaking IM. Finally, a comprehensive set of structural vulnerability functions is assembled by combining the fragility functions with suitable damage-to-loss ratios. We detail each step in the following sections.

[1] https://github.com/gem/global_vulnerability_model.

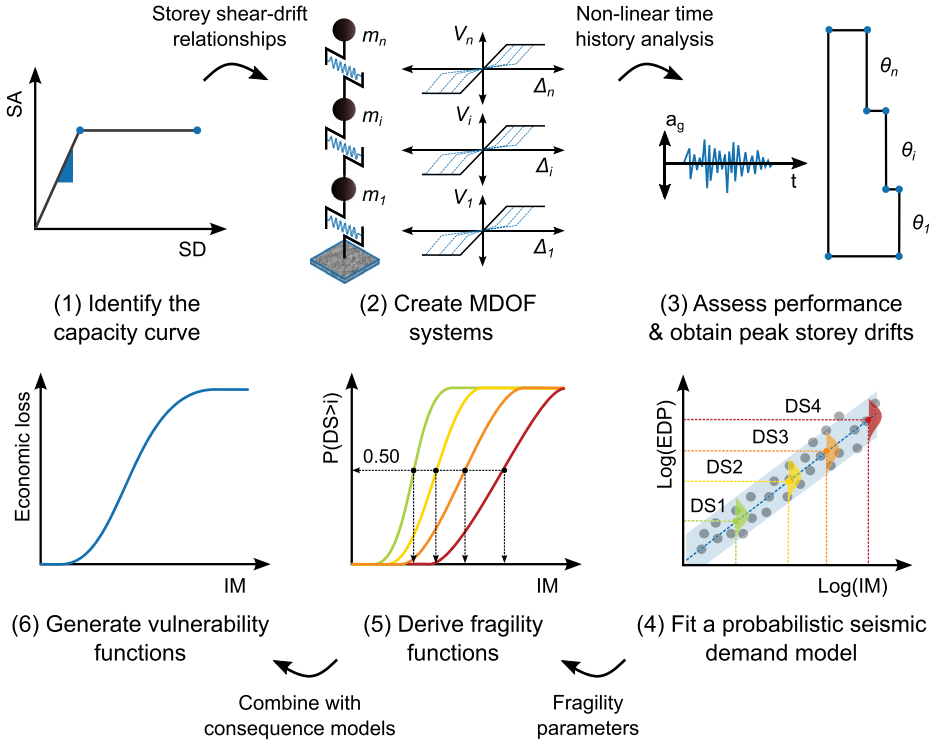



**Fig. 1** Methodology of the derivation of structural fragility and vulnerability functions

## 2.1 Definition of building classes and capacity curves

The new vulnerability database expands the building classes to almost 1,000, designed to represent diverse construction materials, structural systems, and seismic performance levels worldwide. As summarised in Table 1, buildings are categorised based on primary construction materials, lateral load-resisting systems, seismic design code, ductility levels, height (i.e., number of storeys), and occupancy type. Additional attributes can be incorporated to capture regional or structural variations that may affect seismic behaviour, such as the dominant inelastic mechanisms and floor type. Each building class is encoded using a unique taxonomy string that combines these attributes following GEM's taxonomy (Silva et al. 2022). For instance, CR/LFM+CDH+DUM/H:3/RES identifies a three-storey (H:3) reinforced concrete (CR) moment-resisting frame (LFM) with high code design (CDH), moderate ductility (DUM), and residential (RES) occupancy. Further information on all building classes and their global distribution is provided in Yepes-Estrada et al. (2023).

The nonlinear behaviour of each building class is characterised by a capacity curve, which defines its global lateral (shear) strength and deformation capacity. These curves are commonly expressed in the acceleration-displacement response spectrum domain, i.e., spectral displacement ($SD$) versus spectral acceleration ($SA$). To reflect differences in structural nonlinear behaviour, three idealised curve shapes are considered:

**Table 1** Building attributes used to define the building classes in the Global Vulnerability Database

| Attribute | String | Details |
|---|---|---|
| Construction material | CR | Reinforced concrete |
| | EU | Earth construction |
| | INF | Informal construction |
| | MCF | Confined masonry |
| | MR | Reinforced masonry |
| | MUR | Unreinforced masonry |
| | MUR+ADO | Adobe construction |
| | MUR+CBH | Concrete block |
| | MUR+CLBRH | Hollow clay brick |
| | MUR+CLBRS | Solid clay brick |
| | MUR+STDRE | Dressed stone |
| | MUR+STRUB | Rubble stone |
| | S | Steel |
| | S+MCF | Steel and confined masonry |
| | SRC | Concrete composite with steel sections |
| | W | Timber |
| | W+WBB | Bamboo |
| | W+WWD | Wattle and daub |
| Lateral load-resisting system | LDUAL | Dual system |
| | LFINF | Infilled frame |
| | LFM | Moment frame |
| | LPB | Post and beam |
| | LWAL | Wall system |
| | LFBR | Braced frame |
| Code level | CDN | Pre-code |
| | CDL | Low code |
| | CDM | Moderate code |
| | CDH | High code |
| Ductility level | DNO | Non-ductile |
| | DUL | Low ductility |
| | DUM | Moderate ductility |
| | DUH | High ductility |
| Occupancy type | RES | Residential |
| | COM | Commercial |
| | IND | Industrial |
| Height | H | H is followed by the number of storeys |
| Special attributes | NSCA | Non-structural components anchored |
| | VL100 | 100% loss of building volume (e.g., pancake collapse) |
| | CCA | Applicable to buildings in the Caribbean and Central America |
| | SOS | Soft-storey mechanism |
| | FC | Concrete floor |
| | FW | Wood floor |
| | RWO | Wood roof |
| | LC100 | Lateral load coefficient 100% |

- **Bilinear curves** for buildings that experience negligible elastic stiffness degradation and no significant post-yield loss of lateral strength (e.g., steel and timber frames).
- **Trilinear curves** for buildings that exhibit an initial reduction in elastic stiffness due to cracking while maintaining a relatively stable post-yield lateral strength (e.g., reinforced concrete bare frames, dual systems, unreinforced masonry).

- **Quadrilinear curves** for structures that undergo a substantial reduction in lateral strength at large deformation levels (e.g., reinforced concrete infilled frames).

Figure 2 shows the three idealised capacity-curve shapes. $\mathrm{SD}_y$ and $\mathrm{SA}_y$ denote the spectral displacement and acceleration at the global yielding stage, respectively, $\mathrm{SD}_u$ is the ultimate spectral displacement, $\mathrm{T}_1$ is the first-mode vibration period, and $\mathrm{T}_y$ is the vibration period at yielding. The mathematical relationship between $SA$, $SD$, and $T$ used to define the capacity curve for each building class is given in Eq. (1).

$$SA = SD\left(\frac{2\pi}{T}\right)^2 \tag{1}$$

The Martins and Silva (2021) database provided capacity curves for nearly 500 building classes. Here, we expand this coverage to a substantially broader set of classes, spanning additional construction materials, structural systems, heights, seismic code/ductility levels. The capacity curves of the new classes are compiled using evidence from analytical and empirical studies, observations from experimental campaigns, and, where direct data are limited, via engineering judgement drawing on the authors' experience and input from local specialists involved in the long-term development and testing of the original database. Table 2 lists the main references from which the new capacity curves are sourced.

The capacity curves from the studies in Table 2 serve as base prototypes from which new building classes are derived to account for additional heights and ductility levels through a consistent scaling procedure. For each base class, $\mathrm{T}_y$ is first evaluated for the desired new building height based on empirical formulae from the literature (e.g., Crowley and Pinho 2006). Where such formulae are unavailable, $\mathrm{T}_y$ is assumed equal to 1.5 $\mathrm{T}_1$ (Calvi et al. 2006). $\mathrm{SD}_u$ is then computed by reducing the ultimate drift of the base class to account for second-order effects (P-delta) at greater heights using modification factors deduced from existing studies (FEMA 2012a; Crowley et al. 2021; Romão et al. 2021). Similarly, the yield drift is scaled to reflect its dependence on building height and to estimate the corresponding $\mathrm{SD}_y$. Equation (1) is finally used to compute the remaining $SA$ values and construct the full capacity curve for each derived building class. Further ductility levels are incorporated in the same manner by modifying the yield and ultimate drifts of the base class and then repeating the same steps. Figure 3 displays the counts of all building classes, classified by their primary construction material and height category. All adopted capacity curves are documented in the GitHub repository.

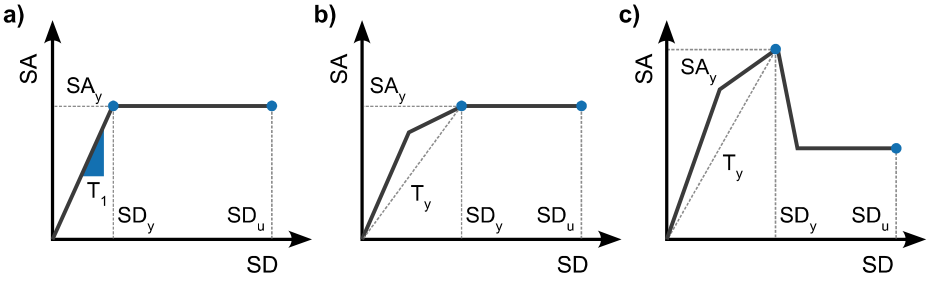



**Fig. 2** Idealised shapes of capacity curves: (**a**) Bilinear; (**b**) Trilinear; and (**c**) Quadrilinear

**Table 2** References for the capacity curves used to describe the nonlinear behaviour of different building classes

| Primary Material of the Building Class | Literature references |
|---|---|
| Adobe and Rammed Earth | (Tarque et al. 2012; Villar-Vega et al. 2017; Lang et al. 2018; Karanikoloudis and Lourenço 2018; Silveira et al. 2018; Battaglia et al. 2021) |
| Unreinforced Masonry | (Barbat et al. 2006; Borzi et al. 2008; Villar-Vega et al. 2017; Lang et al. 2018) |
| Reinforced Masonry | (Voon and Ingham 2006; Shedid et al. 2008; Haach et al. 2010; Murcia-Delso and Shing 2012; Lotfy et al. 2022; FEMA 2024a) |
| Confined Masonry | (Magenes and Calvi 1992; Nucera et al. 2012; Erkoseoglu et al. 2014; Perez Gavilan et al. 2015; Villar-Vega et al. 2017; Ahmed et al. 2018) |
| Reinforced Concrete | (Crowley et al. 2008; Bal et al. 2010; Ricci et al. 2011; Tischer et al. 2012; Villar-Vega et al. 2017; Lang et al. 2018; Tarquini et al. 2019; Parra et al. 2019; Ugalde et al. 2019; Aljawhari et al. 2020; Suzuki and Iervolino 2020; Ugalde and Lopez-Garcia 2020; Farsangi et al. 2021; Gondaliya et al. 2023; FEMA 2024b; Nafeh and O'Reilly 2024) |
| Steel Structures | (Sabelli et al. 2003; McCormick et al. 2007; Tasnimi and Mohebkhah 2011; Ramirez et al. 2012; Radnić et al. 2013; Markulak et al. 2013; Abou-Elfath et al. 2017; Eladly 2017; Del Carpio R. et al. 2019; Jouneghani and Haghollahi 2020; FEMA 2024a) |
| Timber Structures | (Goda and Atkinson 2011; Loss et al. 2013; Villar-Vega et al. 2017; Lang et al. 2018; FEMA 2024a) |

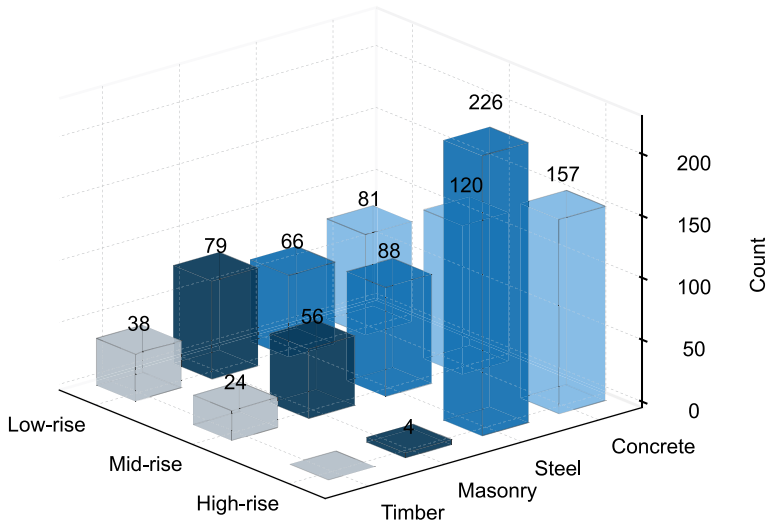



**Fig. 3** Building class counts based on primary construction material and height category

### 2.2 Numerical modelling strategy

Unlike the original vulnerability database of Martins and Silva (2021) that relied on SDOF oscillators, the new version adopts *stick-and-mass* MDOF systems with masses lumped at floor levels and connected by nonlinear springs defining the storey-shear force versus drift behaviour (see Fig. 4). These models account for higher-mode contributions and inelastic demand concentrations, offering a more realistic representation of seismic response and an improved characterisation of structural damage. They also explicitly capture storey-level demands like PSD and PFA, which are necessary to derive vulnerability functions for non-structural components and building contents, as described in Part II of our study (Nafeh et al. 2026b). Although torsional modes are not simulated and storey response is assumed shear-dominated, prior studies have shown that such MDOF systems achieve a favourable balance between reliability and computational efficiency for large-scale seismic risk applications (Lu et al. 2014; Gaetani d'Aragona et al. 2020).

To create the *stick-and-mass* MDOF systems for each building class, the capacity curves introduced in Sect. 2.1 are used as a starting point. While these curves are generally sufficient for an equivalent SDOF representation, their use in MDOF modelling requires conversion to pushover curves relating a building's roof displacement ( $u_{roof}$) to base shear ( $V_{base}$). The conversion follows the principles of structural dynamics as per Eqs. (2) and (3), where $\Gamma_1$ is the first-mode participation factor and $m_{SDOF}$ is the effective mass of the SDOF oscillator, taken equal to 1.0 tonne.

$$u_{roof} = SD\,\Gamma_1 \tag{2}$$

$$V_{base} = SA\,\Gamma_1\, m_{SDOF} \tag{3}$$

The mass of the MDOF system can now be computed via Eq. (4), derived on the basis that $m_{SDOF}$ is equal to 1.0 tonne. It is expressed as a diagonal matrix, $[M] = \mathrm{diag}(m_1, \ldots, m_n)$, where $m_i$ denotes the mass lumped at floor level $i$ out of $n$ floors. $[W] = \mathrm{diag}(w_1, \ldots, w_n)$ is a diagonal weighting matrix whose diagonal terms $w_i$ define the relative mass distribution (profile) across the $n$ floors. For a uniform mass profile (equal mass at each floor), $w_i = 1.0$ for all $i$. $\bar{J}$ is a unity vector of length $n$; $\phi_1$ is the first-mode shape of the building; and $\phi_1^T$ is its transpose.

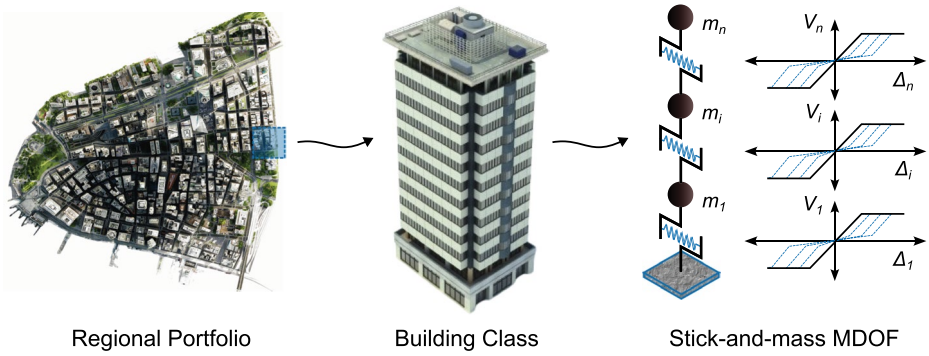



**Fig. 4** Building class to stick-and-mass model idealisation

$$[M] = \frac{\phi_1^T [W] \phi_1}{\left(\phi_1^T [W] \bar{J}\right)^2} [W] \tag{4}$$

The value of $\phi_1$ is obtained through eigenvalue analysis, adopting a uniform storey stiffness and a mass profile with equal floor masses except at the roof, where the mass is decreased by 25% (i.e., $w_n = 0.75$ and $w_i = 1.0$ for $i = 1, \ldots, n-1$). For buildings exhibiting soft-storey behaviour, the stiffness of the first storey is reduced by 80% to reproduce the associated demand concentration (Vijayanarayanan et al. 2017). For bare-frame structures without walls/infills, Eurocode 1-Part 4 (EN 1991-1-4 2004) recommends $\phi_{1,i} = (i/n)^{0.6}$, where $i$ is the floor level index. The shear force-drift relationship is finally proportioned for each storey based on $\phi_1$, following Lu et al. (2014), as per Eqs. (5) and (6). $V_k$ and $\Delta_k$ are the shear force and drift values for storey $k$; $\phi_{1,i}$ is the first-mode ordinate at floor $i$. Eqs. (2)-(6) assume that $\phi_1$ is normalised such that $\phi_{1,n} = 1.0$ (the roof ordinate).

$$V_k = V_{base} \frac{\sum_{j=k}^{n} \phi_{1,j} m_j}{\sum_{i=1}^{n} \phi_{1,i} m_i} \tag{5}$$

$$\Delta_k = (\phi_{1,k} - \phi_{1,k-1})\, u_{roof} \tag{6}$$

Figure 5 illustrates examples of pushover curves for both the equivalent SDOF and adopted MDOF systems, together with the storey-level $V_k - \Delta_k$ relationships used to define the MDOF nonlinear springs. Two three-storey building classes are shown for comparison: (1) a low-code reinforced concrete dual frame system with low ductility (CR/LDUAL/CDL+DUL/H:3); and (2) a moderate-code reinforced concrete infilled frame with low ductility (CR/LFINF/CDM+DUL/H:3).

All MDOF systems are modelled in OpenSeesPy (McKenna 2011). Nonlinear springs connecting mass nodes are assigned the "*Pinching4*" material to reproduce storey-level $V_k - \Delta_k$ relationships. Models adopt Rayleigh damping (Zareian and Medina 2010; Gentile and Galasso 2021), with mass- and stiffness-proportional coefficients calibrated so that

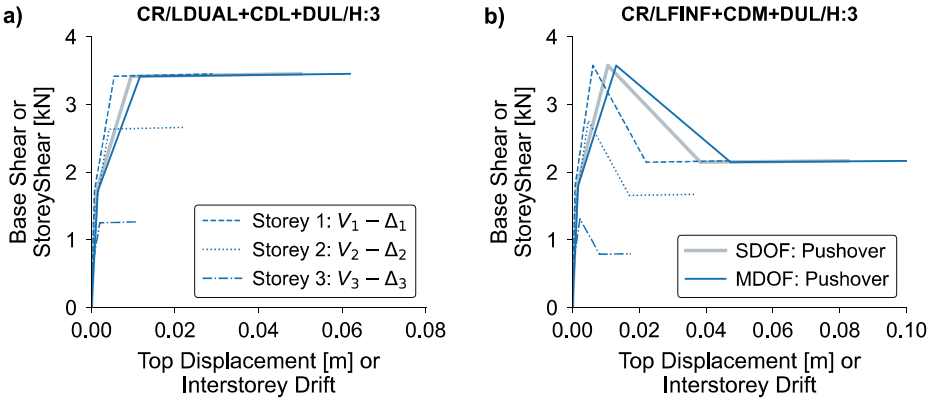



**Fig. 5** SDOF/MDOF pushover and storey-level $V_i$- $\Delta_i$ for: (**a**) Three-storey low code reinforced concrete dual system with low ductility; and (**b**) Three-storey moderate code reinforced concrete infilled frame with low ductility

the first and second modes match the damping ratios prescribed in Martins and Silva (2021) for each building class (i.e., 5% for reinforced concrete and timber, 7.5% for confined masonry, 10% for reinforced and unreinforced masonry, and 3% for steel structures).

### 2.3 Cloud analysis and ground-motion selection

Deriving fragility and vulnerability functions typically involves NLTHA to characterise nonlinear building response across different ground-shaking intensity levels. Several approaches exist in the literature for carrying out NLTHA, like incremental dynamic (Vamvatsikos and Cornell 2002) and multiple stripe (Jalayer and Cornell 2009) analyses. This study adopts the cloud analysis approach (Jalayer et al. 2015), in which buildings are subjected to a set of (usually) unscaled ground-motion records. This choice is well-suited to regional risk assessments as it relies on "as-recorded" ground motions, thereby avoiding statistical bias due to scaling (Dávalos and Miranda 2019; Nafeh and O'Reilly 2022). It is also computationally efficient since it does not require site-specific, hazard-consistent record selection, unlike multiple stripe analysis, for example.

This study advances the original vulnerability database of Martins and Silva (2021) by assembling a more comprehensive, globally representative ground-motion dataset. From over 3,500 accelerograms, a subset of 700 records is selected, spanning various tectonic regimes, including active shallow, stable continental, and subduction zones, which can influence ground-shaking properties (e.g., duration, frequency content). The dataset integrates records from major databases: NGA-West (Bozorgnia et al. 2014), NGA-East (Goulet et al. 2021), NGA-Sub (Bozorgnia et al. 2022), KiK-Net (National Research Institute for Earth Science and Disaster Resilience 2019) and the Engineering Strong Motion Database (Luzi et al. 2020). Figure 6 shows the geographic distribution of the recording stations and tectonic regimes of the selected records.

The ground-shaking intensity of the selected records is characterised through several IM types tailored to the dynamic properties of the building classes. These include specifically: (1) peak ground acceleration (PGA) for low-rise structures; (2) 5%-damped spectral acceleration, $SA\,(T)$, evaluated at representative vibration periods (0.3s for some low- and mid-rise classes, 0.6s for mid-rise classes, and 1.0s for high-rise classes); and (3) average

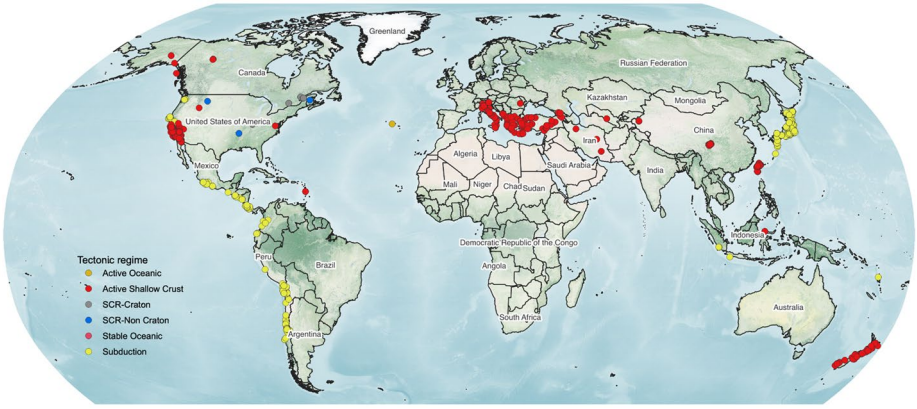



**Fig. 6** Geospatial locations and tectonic regimes of the recording stations

spectral acceleration ( $AvgSA$) (e.g., Eads et al. 2015; Heresi and Miranda 2021; Aljawhari et al. 2025), defined as the geometric mean of ten equally-spaced $SA$ values within a period range 0.1–1.0 s. Compared to conventional IMs like $SA\,(T)$ or PGA, $AvgSA$ has been shown to improve efficiency, sufficiency, and to reduce bias in seismic response estimation (e.g., O'Reilly 2021).

To ensure that the selected records have adequate coverage of a wide range of shaking intensities, the >3,500 candidate motions are distributed into equal-acceleration bins for each IM type. A subset of 700 records is then randomly selected subject to two constraints: (1) a minimum intensity of 0.05 g to maintain engineering relevance; and (2) at least ten records per bin. A small number of records are amplitude-scaled by factors not exceeding 2.5 (records scaled by a factor>2.0 are less than 10%) to supplement the highest-intensity bins and populate damage realisations, particularly for code-compliant building classes. This cap aligns with published recommendations aimed at limiting scaling bias (e.g., Dávalos and Miranda 2019; Nafeh and O'Reilly 2022; Fayaz et al. 2023). It should be noted that amplitude scaling preserves record duration but does not guarantee hazard-consistent spectral shapes across periods and may distort frequency content, which can influence high-rise buildings, whose response is notably sensitive to low-frequency (long-period) content.

Figure 7 depicts the distribution of ground-shaking intensities for the selected IMs. Figure 8 further presents the 5%-damped acceleration response spectra of individual records and the corresponding mean spectrum. The compiled record set, along with the associated metadata, is available in the GitHub repository, and a summary of main record properties (e.g., event magnitude, Joyner-Boore distance, shear-wave velocity, IM value, scaling factor) is provided in the Supplementary Information.

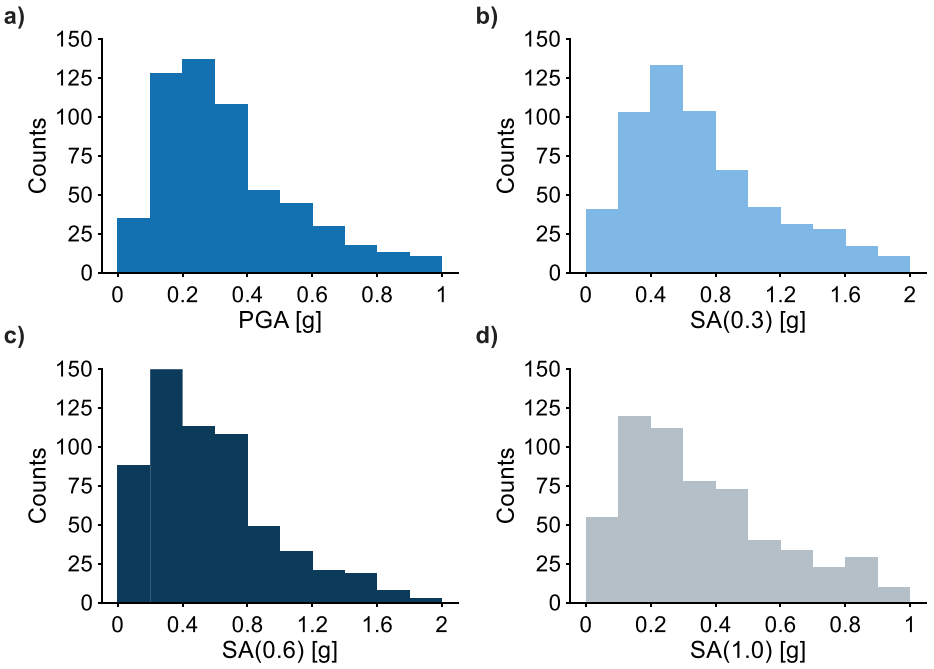



**Fig. 7** Ground-shaking intensity distribution for: (**a**) PGA; (**b**) $SA\,(0.3)$; (**c**) $SA\,(0.6)$; and (**d**) $SA\,(1.0)$

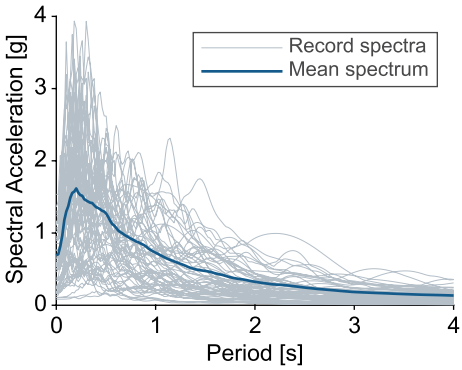



**Fig. 8** 5%-damped acceleration response spectra for individual records and the mean spectrum

### 2.4 Definition of damage states (DSs) and fragility derivation

Structural fragility functions are derived for each building class to describe the probability of exceeding a set of damage states, DSs, over a range of IM levels. Four DSs are considered: slight (DS1), moderate (DS2), extensive (DS3), and complete (DS4). The onset of these structural DSs is inferred numerically through nonlinear analysis, particularly when a selected engineering demand parameter (EDP) in the analysed building attains pre-defined thresholds. In this study, the EDP is the maximum interstorey drift ratio ($\theta_{max}$) (e.g., Raghunandan et al. 2015; Aljawhari et al. 2022), which is strongly correlated with global structural damage, at least for drift-sensitive components. It is acknowledged though that several building components, especially non-structural ones, are sensitive to PFA rather than $\theta_{max}$; this aspect is addressed in Part II (Nafeh et al. 2026b).

In the original Martins and Silva (2021) database, DS thresholds for the SDOF oscillators are defined at specific $SD$ points along the capacity curve: DS1 is mapped at $SD_y$; DS2 at $0.67\,SD_y + 0.33\,SD_u$; DS3 at $0.33\,SD_y + 0.67\,SD_u$; and DS4 at $SD_u$. To transfer these thresholds to the MDOF framework, they are first converted into the corresponding roof displacements, $u_{roof}$, of the MDOF system. The interstorey drift profile at the onset of each DS is then derived using the structural-dynamics relationships outlined in Sect. 2.2, from which the $\theta_{max}$ is taken as the maximum drift across all storeys. This procedure is explained in Table 3, where $SD_y$, $SD_u$, $\Gamma_1$, and $\phi_{1,i}$ are defined earlier, and $h_i$ is the storey height below floor $i$. The process is also visualised in Fig. 9.

Fragility functions are derived via cloud analysis, in which NLTHA is conducted to produce a set of response observations (IM-EDP pairs). A probabilistic seismic demand model is then fitted to these data using a power-law relation in Eq. (7), where $E[EDP]$ is the

**Table 3** DS thresholds for MDOF systems expressed in terms of $\theta_{max}$

| Damage State | Maximum Interstorey Drift Ratio Thresholds |
|---|---|
| Slight (DS1) | $\theta_{max,DS1} = \max_{i=1,\ldots,n} \left[\Gamma_1(\phi_{1,i} - \phi_{1,i-1})\, SD_y/h_i\right]$ |
| Moderate (DS2) | $\theta_{max,DS2} = \max_{i=1,\ldots,n} \left[\Gamma_1(\phi_{1,i} - \phi_{1,i-1})(0.67\, SD_y + 0.33\, SD_u)/h_i\right]$ |
| Extensive (DS3) | $\theta_{max,DS3} = \max_{i=1,\ldots,n} \left[\Gamma_1(\phi_{1,i} - \phi_{1,i-1})(0.33\, SD_y + 0.67\, SD_u)/h_i\right]$ |
| Complete (DS4) | $\theta_{max,DS4} = \max_{i=1,\ldots,n} \left[\Gamma_1(\phi_{1,i} - \phi_{1,i-1})\, SD_u/h_i\right]$ |

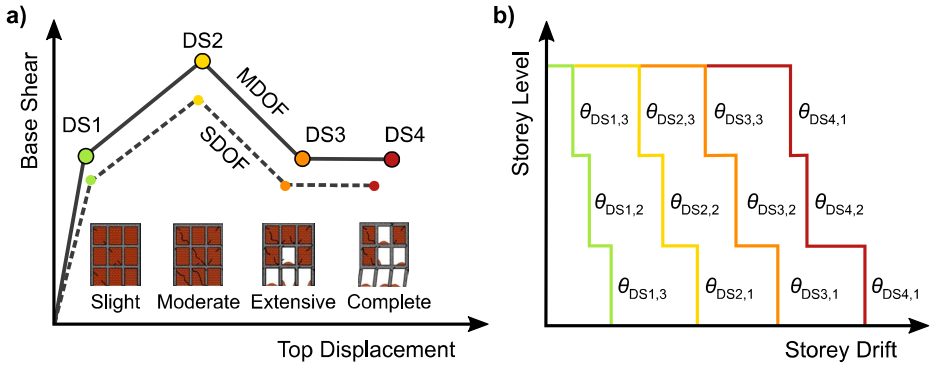



**Fig. 9** Derivation of DS thresholds for MDOF systems: (**a**) Pushover results; (**b**) Interstorey drift profile

expected EDP value and $a$ and $b$ are regression parameters (see Fig. 10). The dispersion term reflecting record-to-record response variability ( $\beta_{rec}$) is defined by Eq. (8), where $k$ is the number of records, and $EDP_i$ is the EDP produced by record $i$. To account for the additional uncertainty due to building-to-building variability (and modelling idealisations), an extra dispersion component ( $\beta_{bldg}$) is included, taken as 0.30 following previous studies (e.g., FEMA 2012b). Future refinements could reduce this epistemic component by calibrating against real damage/loss data for consistent building types, or by explicitly modelling building-to-building variability through randomised capacity-curve parameters rather than deterministic inputs. The total dispersion ( $\beta$ ) is finally computed by combining $\beta_{rec}$ and $\beta_{bldg}$, as per Eq. (9).

$$E\left[EDP\right] = aIM^b \tag{7}$$

$$\beta_{rec} = \sqrt{\frac{\sum_{i=1}^{k}\left(\ln EDP_i - E\left[\ln EDP\right]\right)^2}{k-2}} \tag{8}$$

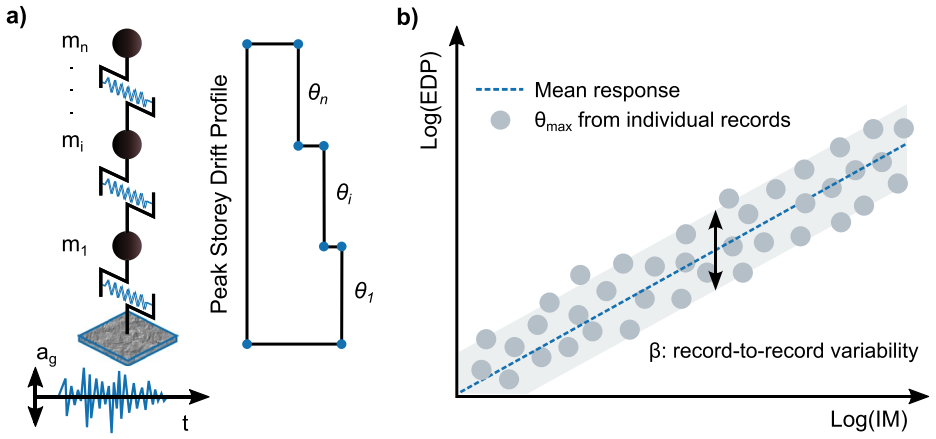



**Fig. 10** (**a**) Idealised *stick-and-mass* MDOF model with PSD demands evaluated via NLTHA; and (**b**) Cloud analysis with fitted probabilistic seismic demand model

$$\beta = \sqrt{{\beta_{rec}}^2 + {\beta_{bldg}}^2} \tag{9}$$

To estimate the power-law regression parameters $a$ and $b$ in Eq. (7), the maximum likelihood method (Stafford 2008; Lallemant et al. 2015) is used. It identifies the parameter values that maximise the likelihood of the NLTHA observations (i.e., $EDP_i$), given the corresponding IM values, according to Eq. (10). $\phi(\bullet)$ is the probability density function of the standard normal distribution.

$$L = \prod_{i=1}^{k} \left[ \phi \left( \frac{EDP_i - a - bIM_i}{\beta} \right) \right] \tag{10}$$

Fitting the power law is straightforward in principle, but the regression can be biased by extreme NLTHA outcomes (i.e., excessively large drifts/accelerations due to numerical instability near collapse). If retained, these outliers can unduly influence the fitted parameters and inflate predicted damage, especially at high IM levels. To mitigate this effect, a "censored" regression procedure is adopted, in which response observations exceeding a censoring threshold, $EDP_c$, are treated as collapses. Based on Martins and Silva (2021), $EDP_c$ is set as 1.5 times the EDP associated with DS4 (i.e., $\theta_{max,DS4}$). The NLTHA results are accordingly split into $n_0$ uncensored and $n_c$ censored observations. For the uncensored subset, the likelihood function is given by Eq. (10), whereas for the censored subset, the contribution is expressed as the complementary probability of exceeding $EDP_c$. The resulting combined log-likelihood function is reported in Eq. (11) (Stafford 2008), where $\Phi(\bullet)$ is the cumulative distribution function of the standard normal distribution.

$$\ln(L) = \sum_{i=1}^{n_0} \ln \phi \left( \frac{EDP_i - a - bIM_i}{\beta} \right) + \sum_{j=1}^{n_c} \ln \left[ 1 - \Phi \left( \frac{EDP_c - a - bIM_j}{\beta} \right) \right] \tag{11}$$

Once the power-law model is fitted, fragility functions can be derived for all DSs. These are represented as a lognormal cumulative distribution function (Porter et al. 2007; Eads et al. 2013), as per Eq. (12), which defines the probability that a particular DS is exceeded, given an IM level. $\mu_{DSi}$ is the median IM corresponding to the exceedance of the "i-th" DS ($DSi$). $\beta$ and $\Phi(\bullet)$ were defined previously. To express the dispersion in the IM space consistently with Eq. (12), $\beta_{rec}$ must first be divided by the regression parameter $b$ before computing the value of $\beta$.

$$P(DS \geq DSi|IM) = \Phi \left( \frac{ln(IM/\mu_{DSi})}{\beta} \right) \tag{12}$$

### 2.5 Derivation of vulnerability functions

Vulnerability functions quantify the economic loss ratio (repair cost of damaged structural components normalised by their replacement cost) over a range of IM levels. They are gen-

**Table 4** Selected damage-to-loss ratios for each DS

| Damage State | Mean damage-to-loss ratio |
|---|---|
| Slight (DS1) | 0.05 |
| Moderate (DS2) | 0.15 |
| Extensive (DS3) | 0.60 |
| Complete (DS4) | 1.00 |

erated by combining the DS probabilities from fragility functions (Sect. 2.4) with adequate damage-to-loss ratios through the total probability theorem, according to Eq. (13).

$$E(LR|IM) = \sum_{i=1}^{n_{DS}} P\left(DS = DSi|IM\right) DLR_{DSi} \tag{13}$$

Where $E\left(LR|\,IM\right)$ is the expected structural loss ratio conditioned on an IM level; $P\left(DS = DSi|IM\right)$ is the probability that the building is in $DSi$ at that IM level; $DLR_{DSi}$ is the damage-to-loss ratio associated with $DSi$; and $n_{DS}$ is the number of DSs. The variability of $E\left(LR|\,IM\right)$ is captured using the method proposed by Silva (Silva 2019), who examined the influence of record-to-record variability on the dispersion of loss ratios for different building classes. The selected $DLR_{DSi}$ values are consistent with studies in the literature, derived using either empirical data (e.g., Di Pasquale et al. 2005; Bal et al. 2008) or analytical procedures (e.g., Martins et al. 2016; Aljawhari et al. 2023, 2025). The mean $DLR_{DSi}$ for each DS is provided in Table 4. A limitation of this vulnerability derivation approach is that a single $DLR_{DSi}$ is applied to the entire building for a given DS, which might overestimate losses when damage is concentrated in a localised subset of storeys (e.g., some high-rise buildings, soft-storey mechanisms).

### 2.6 Integration with the OQ-VMTK package

The numerical modelling and analysis workflows presented herein are fully automated through the new version of "OpenQuake's Vulnerability Modellers Toolkit" (OQ-VMTK), an open-source Python package that imports SDOF capacity-curve information and transforms it into the corresponding *stick-and-mass* MDOF system. The toolkit streamlines essential modelling tasks, including the assignment of nodes, masses, boundary conditions, nonlinear springs, and damping, as well as the execution of various analysis types (e.g., gravity, modal, nonlinear static, nonlinear cyclic, and NLTHA using user-specified records). OQ-VMTK further incorporates modules that automate the derivation of fragility functions adopting different methods, in addition to vulnerability functions for a range of seismic consequences (e.g., economic losses in structural and non-structural components, content losses, fatalities, collapses). High-quality data visualisation is also supported through a dedicated plotting module. OQ-VMTK is freely accessible on GitHub[2], allowing the scientific community to reproduce the models and results described here and to develop models for building classes not yet covered in this study. Users are referred to Nafeh et al. (2026a) for a detailed description of OQ-VMTK.

[2] https://github.com/GEMScienceTools/oq-vmtk.

## 3 End-to-end application: results and discussion

### 3.1 Sample fragility and vulnerability functions

Given the large number of building classes analysed in this study, only selected results are reported here to emphasise the most informative trends. The complete results and datasets are accessible via GitHub. Table 5 summarises the fitted parameters of structural fragility functions (median, $\mu_{DSi}$, and dispersion, $\beta$) for globally representative building classes. They differ in height (H) and include reinforced concrete frames with masonry infills (CR/LFINF), several unreinforced masonry (MUR) typologies, and steel frames with shear walls (S/LWAL). For each class, the most efficient IM is selected, defined as the one that minimises record-to-record variability (i.e., yields the lowest $\beta_{rec}$).

The results show clear dependencies on both design code and ductility. Buildings with high code (CDH) and high ductility (DUH) have $\mu_{DSi}$ values up to nearly twice those of their low code (CDL) and low ductility (DUL) counterparts. The influence of primary construction material and lateral load-resisting system is also evident. S/LWAL buildings consistently exhibit the largest $\mu_{DSi}$ values, implying the lowest susceptibility to structural

**Table 5** Parameters of structural fragility functions: median ($\mu_{DSi}$) and dispersion ($\beta$) for sample building classes

| Building class | Efficient IM | $\mu_{DS1}$ [g] | $\mu_{DS2}$ [g] | $\mu_{DS3}$ [g] | $\mu_{DS4}$ [g] | $\beta$ |
|---|---|---|---|---|---|---|
| CR/LFINF+CDH+DUH/H:3 | SA (0.3) | 1.367 | 1.990 | 2.482 | 2.886 | 0.446 |
| CR/LFINF+CDH+DUM/H:3 | SA (0.3) | 1.198 | 1.706 | 2.106 | 2.434 | 0.456 |
| CR/LFINF+CDM+DUM/H:3 | SA (0.3) | 0.900 | 1.270 | 1.574 | 1.827 | 0.496 |
| CR/LFINF+CDM+DUL/H:3 | SA (0.3) | 0.721 | 0.978 | 1.191 | 1.369 | 0.510 |
| CR/LFINF+CDL+DUL/H:3 | SA (0.6) | 0.364 | 0.497 | 0.608 | 0.703 | 0.467 |
| CR/LFINF+CDN+DNO/H:3 | SA (0.6) | 0.273 | 0.360 | 0.435 | 0.500 | 0.470 |
| CR/LFINF+CDH+DUH/H:8 | SA (0.6) | 0.757 | 0.975 | 1.170 | 1.340 | 0.480 |
| CR/LFINF+CDH+DUM/H:8 | SA (0.6) | 0.662 | 0.842 | 1.003 | 1.144 | 0.490 |
| CR/LFINF+CDM+DUM/H:8 | SA (1.0) | 0.354 | 0.441 | 0.520 | 0.590 | 0.463 |
| CR/LFINF+CDM+DUL/H:8 | SA (1.0) | 0.279 | 0.328 | 0.373 | 0.414 | 0.471 |
| CR/LFINF+CDL+DUL/H:8 | SA (1.0) | 0.209 | 0.243 | 0.275 | 0.305 | 0.500 |
| CR/LFINF+CDN+DNO/H:8 | SA (1.0) | 0.125 | 0.158 | 0.187 | 0.213 | 0.521 |
| S/LWAL+CDH+DUH/H:7 | SA (0.3) | 1.183 | 2.033 | 2.671 | 3.187 | 0.452 |
| S/LWAL+CDH+DUM/H:7 | SA (0.3) | 1.034 | 1.774 | 2.329 | 2.779 | 0.473 |
| S/LWAL+CDM+DUM/H:7 | SA (0.3) | 0.881 | 1.315 | 1.649 | 1.921 | 0.477 |
| S/LWAL+CDM+DUL/H:7 | SA (0.3) | 0.752 | 1.030 | 1.247 | 1.424 | 0.457 |
| S/LWAL+CDL+DUM/H:7 | SA (0.3) | 0.698 | 0.867 | 1.004 | 1.118 | 0.453 |
| S/LWAL+CDL+DUL/H:7 | SA (0.3) | 0.572 | 0.712 | 0.824 | 0.916 | 0.468 |
| MUR+CBH/LWAL+DNO/H:3 | SA (0.6) | 0.227 | 0.413 | 0.562 | 0.686 | 0.428 |
| MUR+STDRE/LWAL+DNO/H:3 | SA (0.6) | 0.254 | 0.420 | 0.556 | 0.670 | 0.431 |
| MUR+CLBRS/LWAL+DNO/H:3 | SA (0.6) | 0.204 | 0.370 | 0.501 | 0.610 | 0.427 |
| MUR+CLBRH/LWAL+DNO/H:3 | SA (0.6) | 0.177 | 0.332 | 0.453 | 0.552 | 0.428 |
| MUR+STRUB/LWAL+DNO/H:3 | SA (0.6) | 0.204 | 0.342 | 0.453 | 0.545 | 0.427 |
| MUR+ADO/LWAL+DNO/H:3 | SA (0.6) | 0.144 | 0.252 | 0.341 | 0.416 | 0.447 |

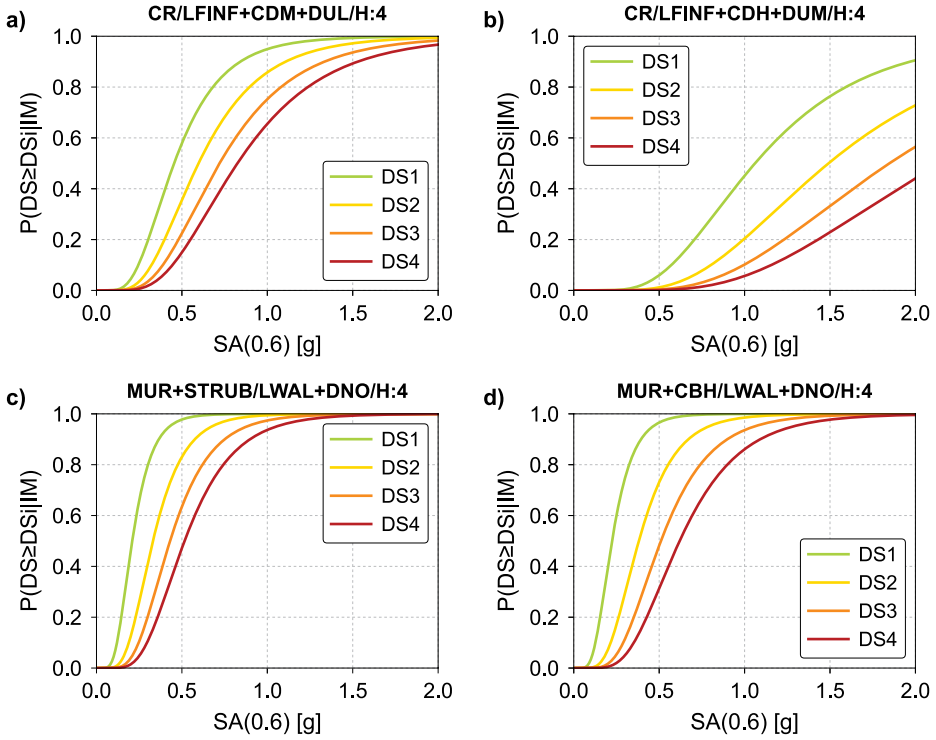



**Fig. 11** Fragility functions for: (**a**) Four-storey reinforced concrete infilled frame with moderate-code/low-ductility; (**b**) Four-storey reinforced concrete infilled frame with high-code/moderate-ductility; (**c**) Four-storey pre-code unreinforced masonry with rubble stone; and (**d**) Four-storey pre-code unreinforced masonry with concrete blocks

damage, followed by CR/LFINF classes. By contrast, MUR classes have the smallest $\mu_{DSi}$, given their limited deformation capacity and brittle failure mechanisms.

To illustrate some of the above trends, Fig. 11 presents structural fragility functions for four building classes with matched heights (H:4) and a common efficient IM to enable a direct cross-class comparison. Figure 11(a-b) show reinforced concrete frames with masonry infills in two design configurations: moderate-code/low-ductility and high-code/moderate-ductility, respectively. Figure 11(c-d) plots the fragilities corresponding to unreinforced masonry buildings, contrasting rubble-stone construction (Fig. 11c) with hollow concrete-block construction (Fig. 11d). The associated vulnerability functions are depicted in Fig. 12, further corroborating the fragility-based observations by highlighting marked differences in expected structural loss ratios across the four classes.

### 3.2 Original versus new global vulnerability database

The new global vulnerability database introduced in this study brings major upgrades over the original Martins and Silva (2021) version. Advancements include the transition from simplified SDOF oscillators to stick-and-mass MDOF systems and the adoption of $\theta_{max}$ as the primary EDP to detect structural damage. Unlike $SD$, which is suited to SDOF oscil-

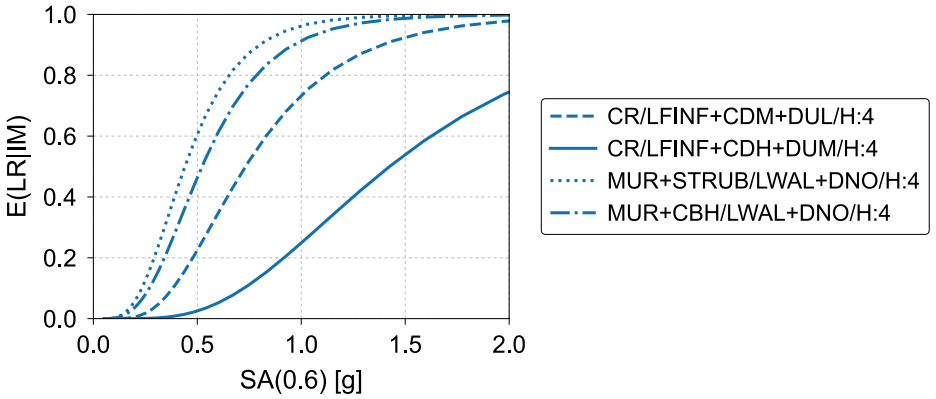



**Fig. 12** Vulnerability functions for selected building classes with similar height

lators, $\theta_{max}$ explicitly reflects storey-level deformations, capturing variations in drift profiles and inelastic demand concentration in multi-storey buildings. As a result, the updated framework provides a more reliable basis for deriving fragility and vulnerability functions, especially for classes whose response cannot be effectively addressed by SDOF oscillators. This section compares the new and the original databases with respect to these functions and discusses potential implications on regional risk assessments.

Figure 13 examines the median values of fragility functions, $\mu_{DSi}$, across different building height ranges by plotting those obtained from the new database on the horizontal axis against those from Martins and Silva (2021) on the vertical axis. For one-storey buildings (Fig. 13a), modelled as SDOF oscillators in both databases, $\mu_{DSi}$ values show slight deviation with an average difference of 15%. This is attributed to the updated ground-motion set that is larger and more globally representative, spans multiple tectonic environments and provides more balanced coverage across IM levels. This means that the new set brings changes in frequency content, duration, and the sampling of damaging motions, which can influence NLTHA response predictions and, in turn, the fitted probabilistic seis-

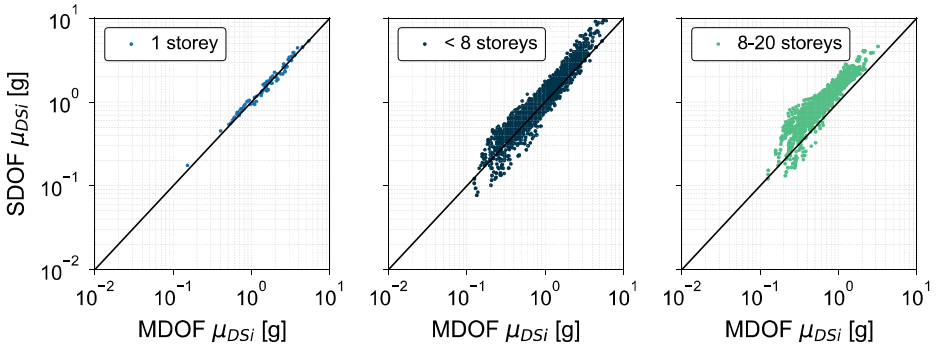



**Fig. 13** Comparing the new and original version of GEM database in terms of median fragility, $\mu_{DSi}$, for these height ranges: (**a**) One-storey; (**b**) Up to 8 storeys; and (**c**) 8–20 storeys. Close agreement is shown for low- to mid-rise structures, while high-rise classes exhibit a significant divergence

mic demand models. This effect is more evident at the upper end of the IM range, where record availability and representativeness play a key role in the stability of cloud-based fits.

For low- to mid-rise buildings up to eight storeys (Fig. 13b), deviations increase, with average differences in $\mu_{DSi}$ reaching 30% due to both the updated modelling strategy and new record set. At the portfolio level, these shifts suggest a moderate impact on regional risk outcomes, given that MDOF models tend to predict larger losses for multi-storey buildings. By contrast, significant discrepancies are observed for high-rise buildings (8–20 storeys; Fig. 13c), where the original database reports $\mu_{DSi}$ that are, on average, 50% larger than those derived here. This stems from the inability of SDOF oscillators to capture higher-mode effects and localised inter-storey demands. Consequently, reliance on SDOF-based fragility for high-rise buildings may lead to considerable risk underestimation.

The above trends are also illustrated in Fig. 14, which compares structural vulnerability functions for a mid-rise (7 storeys) reinforced concrete dual system and a high-rise (35 storeys) concrete shear wall building; both with moderate code and low ductility. For the mid-rise class in Fig. 14(a), the functions from both databases show close agreement. On the contrary, the high-rise comparison in Fig. 14(b) reveals a high divergence. The MDOF-based vulnerability function predicts loss ratios, $LR$, that are up to 2.5 times those calculated through the SDOF-based function.

To further demonstrate how the updated modelling strategy and ground-motion set affect risk-oriented metrics, average annual loss ratios ( $AALR$) are evaluated for a subset of low-, mid-, and high-rise building classes selected based on their prevalence in the global exposure model (Yepes-Estrada et al. 2023). $AALR$ reflects the expected yearly loss due to repairing seismic damage in a building (normalised by its replacement cost), and is obtained by averaging losses over the full range of potential ground-shaking scenarios. $AALR$ provides a single, policy-relevant measure of long-term risk; thus it is widely used by policymakers, insurers, and engineers to prioritise retrofitting strategies, inform resource allocation, and assess the cost-effectiveness of risk-reduction measures.

In this study, $AALR$ is computed by convolving each vulnerability function with a hazard curve that defines the mean annual frequency of exceeding ( $\lambda$ ) different ground-shaking levels (e.g., Gentile and Galasso 2022). This convolution produces a loss curve relating $\lambda$ to different levels of $LR$. The $AALR$ is then obtained as the area under the loss curve,

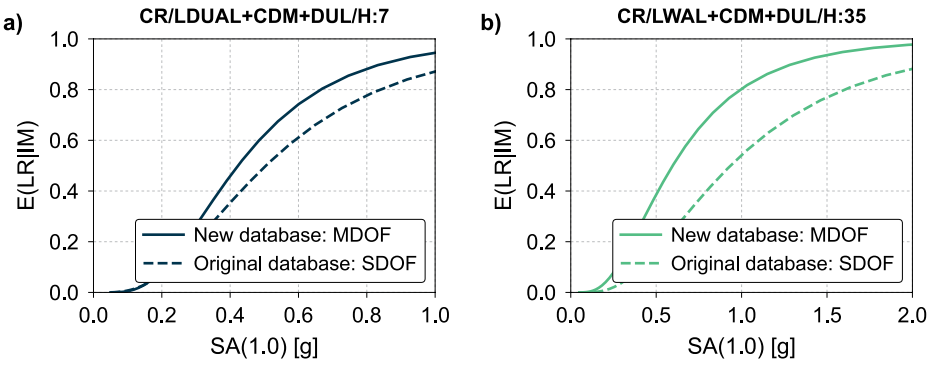



**Fig. 14** Structural vulnerability functions from the new and original databases for: (**a**) 7-storey reinforced concrete dual system; and (**b**) 35-storey concrete shear wall building; both with moderate code and low ductility. Differences are moderate for the mid-rise class and become significant for the high-rise one

as expressed by the integral in Eq. (14). It should be noted that $AALR$ values are sensitive to the $DLR_{DSi}$ adopted to derive vulnerability functions, with particularly strong influence from the lower DSs (i.e., $DLR_{DS1}$ and $DLR_{DS2}$). This reflects the fact that buildings typically incur DS1 and DS2 at low-to-moderate ground-shaking intensities, which occur more frequently and thus have larger contributions to annualised losses.

$$AALR = \int_0^{\infty} LR(\lambda)\, d\lambda \tag{14}$$

Three cities with high seismic activity are adopted as test beds: Wellington (New Zealand), Istanbul (Türkiye), and Los Angeles (USA). Hazard curves for each location and IM type are acquired from GEM's latest hazard mosaic (Johnson et al. 2023). Figure 15 displays the resulting hazard curves (IM versus $\lambda$) assuming rock site conditions.

Figure 16 plots the $AALR$ estimates for the selected low- and mid-rise building classes (<8 storeys), computed using the MDOF- and SDOF-based vulnerability functions. The two databases produce consistent results and variations remain modest across most classes, with average differences ranging between 9% and 26%. This range depends not only on the building class, but also the hazard curve used in the convolution process, particularly because the most efficient IM may differ between the two modelling strategies. Generally, the AALR values derived from MDOF-based vulnerability tend to be relatively larger for multi-storey buildings, echoing the findings drawn from Fig. 13.

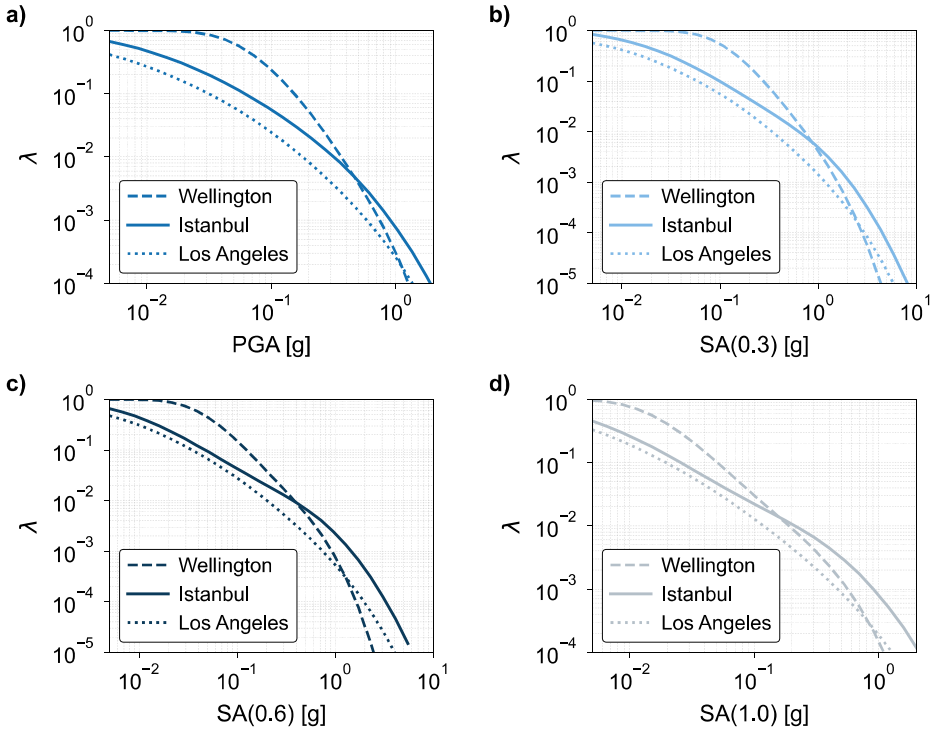



**Fig. 15** Hazard curves for Wellington, Istanbul, and Los Angeles, considering the following IMs: (**a**) PGA; (**b**) $SA\,(0.3)$; (**c**) $SA\,(0.6)$; and (**d**) $SA\,(1.0)$

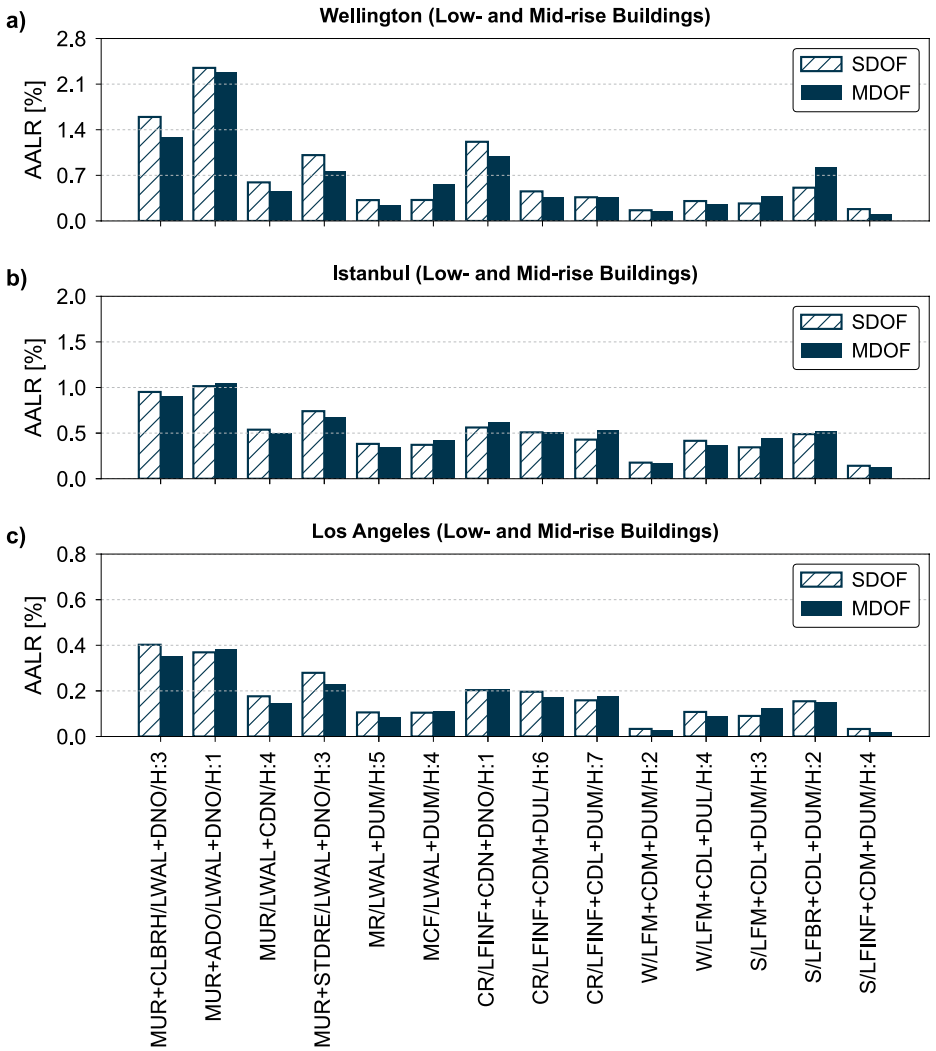



**Fig. 16** Average annual loss ratio, AALR, for low- and mid-rise building classes located in: (**a**) Wellington; (**b**) Istanbul; and (**c**) Los Angeles. Both SDOF- and MDOF-based databases provide consistent AALR values

A similar exercise is carried out for the high-rise sample (>8 storeys). The resulting $AALR$ values are illustrated in Fig. 17, revealing a systematic underestimation of annualised economic losses when SDOF-based vulnerability functions are used. In fact, the updated modelling strategy yields $AALR$ estimates that are 70% to 98% larger (on average), with the exact magnitude varying by building class and by the hazard curve (i.e., city). At portfolio level, seismic loss and risk predictions can be materially amplified in regions experiencing rapid urbanisation and growing stocks of high-rise structures, given

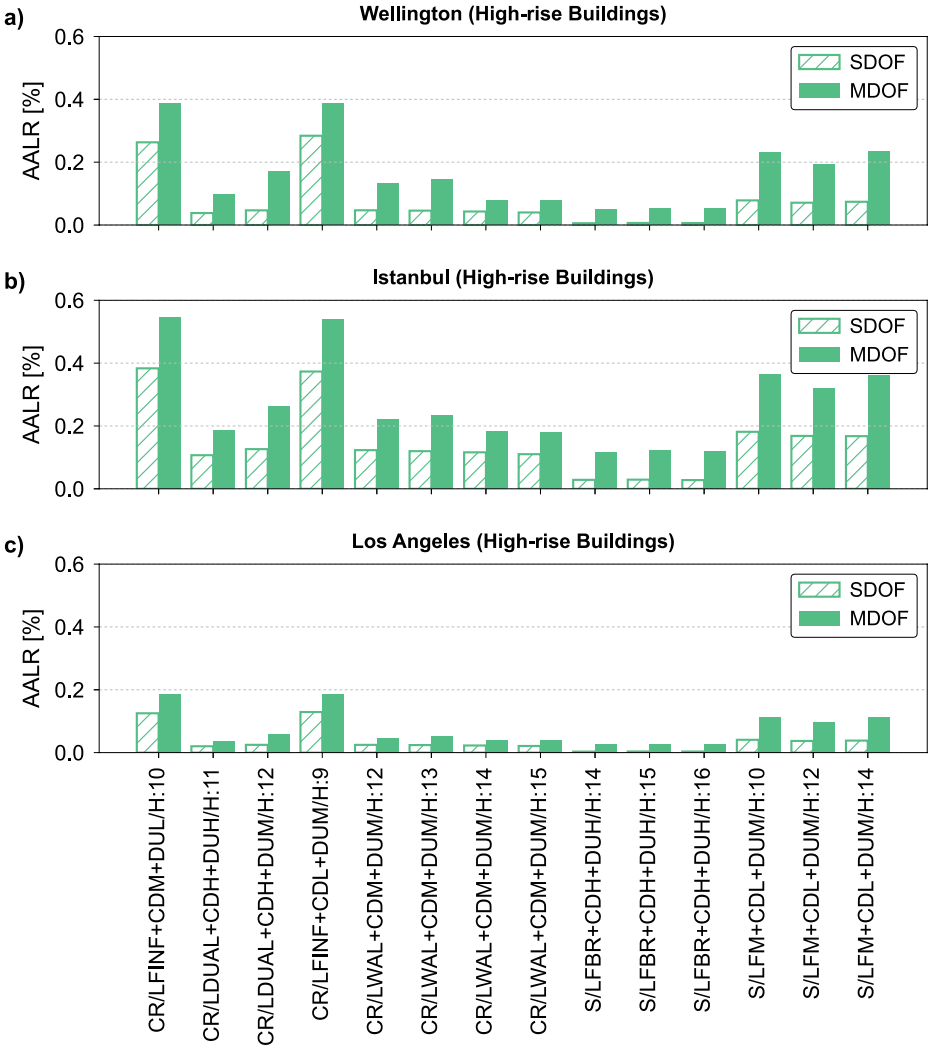



**Fig. 17** Average annual loss ratio, AALR, for high-rise building classes located in: (**a**) Wellington; (**b**) Istanbul; and (**c**) Los Angeles. SDOF-based models systematically underestimate AALR relative to their MDOF counterparts

their larger $AALR$ and replacement cost. This might alter the ranking of retrofitting priorities and influence (re-)insurance pricing, as well as disaster risk financing.

Taken together, the results in this section highlight that modelling choices can substantially affect loss estimates and risk metrics, particularly for tall buildings, and that overly simplified representations may introduce extensive bias into regional risk assessments and the decisions that depend on them.

## 4 Conclusions

This study delivers a new, comprehensive global database that offers seismic vulnerability and fragility functions tailored for (sub-)national, regional, and global risk assessment applications. The new database expands global coverage, compared to the earlier version by Martins and Silva (2021), while improving the physical realism of the underlying structural response simulations via an updated numerical modelling strategy. These developments strengthen the basis for robust risk estimation and support evidence-based disaster-mitigation and resilience planning. The main advancements are:

- Expanded building-class coverage. The database now represents around 1,000 building classes, encompassing a wide range of construction materials, lateral load-resisting systems, code levels, ductility levels, and heights.
- Upgraded numerical modelling. Simplified SDOF oscillators are replaced by efficient *stick-and-mass* MDOF systems that explicitly resolve both storey-level demands (e.g., storey drift, peak floor acceleration) and complex seismic response patterns (e.g., soft storey, higher modes), allowing a better characterisation of damage and loss.
- Broader ground-motion record set. NLTHA was performed using an extensive record set covering several tectonic environments (e.g., subduction, stable continental).
- A new suite of fragility and vulnerability functions providing structural damage and loss predictions. This was derived based on the new MDOF systems.

A comparison between the new vulnerability database and the original one by Martins and Silva (2021) revealed a high consistency in median values of structural fragility functions, $\mu_{DSi}$, for low- and mid-rise structures (up to 8 storeys). In contrast, for high-rise buildings, the original database substantially overestimated the $\mu_{DSi}$ values by 50% in some building classes, reflecting the limitations of SDOF oscillators. Such systems cannot capture higher-mode effects and inelastic demand concentration, which consequently led to underpredictions of structural damage and loss. Similar conclusions could be drawn regarding risk metrics, such as the average annual loss ratio, AALR.

The stick-and-mass MDOF models used in this study are intended for national and regional assessments and therefore incorporate deliberate simplifications. For example, torsional response is not explicitly represented, and the adopted shear building idealisation may be less adequate for classes dominated by other deformation mechanisms (e.g., flexure). The assumed uniform mass profile affects the first-mode shape, and in turn, the allocation of storey shear-drift relationships and the computed storey demands. Such profile might not be appropriate for buildings with pronounced mass irregularity (e.g., podium configurations). Nevertheless, the adopted modelling strategy has proven to be suitable for portfolio applications (Lu et al. 2014; Gaetani d'Aragona et al. 2020). Importantly, users can further refine modelling assumptions with locally representative inputs and regenerate fragility and vulnerability functions via the open-access OQ-VMTK tool (Nafeh et al. 2026a).

Future developments will prioritise: (1) state-dependent fragility and vulnerability functions that account for damage accumulation due to sequential ground shaking; (2) functions addressing the effects of structural retrofit; and (3) tectonic-specific fragility and vulnerability data (e.g., subduction zones, strike-slip faults). Upcoming database releases will also include systematic benchmarking of selected vulnerability functions against observed post-

earthquake damage and loss data, mainly using GEM's Impact Database (GEID) (Karim Zadeh et al. 2025), developed to support validation of earthquake impact (e.g., loss) models. Such benchmarking is expected to be most informative at regional/portfolio scales, given heterogeneity in loss definitions and uncertainties in taxonomy and exposure mapping associated with empirical/observational databases.

The work presented here constitutes Part I of the new Global Vulnerability Model and provides the structural vulnerability component supporting the development of the 2026 version of the Global Seismic Risk Model. A companion paper (Part II) leverages the NLTHA output provided here (i.e., storey-level demands) to quantify additional seismic consequences, particularly damage and economic losses in non-structural components and building contents.

**Acknowledgements** The authors gratefully acknowledge Amir Taherian (University of Aveiro, Portugal) for his valuable contribution to the selection of ground-motion records used for nonlinear analysis in this study.

**Author contributions** All authors contributed to the study conception and design. Material preparation, literature review, modelling, analysis, post-processing, and figure design were performed by KA and AN. All authors contributed to the writing and revision of the manuscript.

**Funding** The authors declare that no funds, grants, or other support were received during the preparation of this manuscript.

**Data availability** The datasets generated during the current study are available in our GitHub repository, https://github.com/gem/global_vulnerability_model.

## Declarations

**Competing interests** The authors have no relevant financial or non-financial interests to disclose.

**Open Access** This article is licensed under a Creative Commons Attribution 4.0 International License, which permits use, sharing, adaptation, distribution and reproduction in any medium or format, as long as you give appropriate credit to the original author(s) and the source, provide a link to the Creative Commons licence, and indicate if changes were made. The images or other third party material in this article are included in the article's Creative Commons licence, unless indicated otherwise in a credit line to the material. If material is not included in the article's Creative Commons licence and your intended use is not permitted by statutory regulation or exceeds the permitted use, you will need to obtain permission directly from the copyright holder. To view a copy of this licence, visit http://creativecommons.org/licenses/by/4.0/.

## References

Abou-Elfath H, Ramadan M, Meshaly M, Fdiel HA (2017) Seismic performance of steel frames designed using different allowable story drift limits. Alexandria Eng J 56:241–249. https://doi.org/10.1016/j.aej.2016.08.028

Ahmed A, Ahmad I, Shahzada K et al (2018) Seismic Capacity Assessment of Confined Brick Masonry Building: An Experimental Approach. Shock Vib 2018. https://doi.org/10.1155/2018/4756352

Aljawhari K, Gentile R, Freddi F, Galasso C (2020) Effects of ground-motion sequences on fragility and vulnerability of case-study reinforced concrete frames. Bull Earthq Eng. https://doi.org/10.1007/s10518-020-01006-8

Aljawhari K, Gentile R, Galasso C (2022) A fragility-oriented approach for seismic retrofit design. Earthq Spectra 38:1813–1843. https://doi.org/10.1177/87552930221078324

Aljawhari K, Gentile R, Galasso C (2023) Simulation-based consequence models of seismic direct loss and repair time for archetype reinforced concrete frames. Soil Dyn Earthq Eng 172:107979. https://doi.org/10.1016/j.soildyn.2023.107979

Aljawhari K, Gentile R, Galasso C (2024) Earthquake-induced environmental impacts for residential Italian buildings: consequence models and risk assessment. J Build Eng 84. https://doi.org/10.1016/j.jobe.2023.108149

Aljawhari K, Gentile R, Galasso C (2025) Beyond Direct Economic Losses: An Integrated Approach to Seismic Retrofit Considering Sustainability and Indirect Losses. Earthq Eng Struct Dyn. https://doi.org/10.1002/eqe.4324

Angelucci G, De Luca F, De Risi R et al (2025) Simplified model for the seismic performance of masonry infilled RC buildings. Eng Struct 342:120903. https://doi.org/10.1016/j.engstruct.2025.120903

Angelucci G, Mollaioli F, Molle M, Paris S (2022) Performance assessment of timber high-rise buildings: structural and technological considerations. Open Constr Build Technol J 16. https://doi.org/10.2174/18748368-v16-e2206270

Bal IE, Crowley H, Pinho R, Gülay FG (2008) Detailed assessment of structural characteristics of Turkish RC building stock for loss assessment models. Soil Dyn Earthq Eng 28:914–932. https://doi.org/10.1016/j.soildyn.2007.10.005

Bal I, Engin C, Helen P, Rui P (2010) Displacement-based earthquake loss assessment: method development and application to Turkish building stock. IUSS Press

Barbat AH, Pujades LG, Lantada N (2006) Performance of Buildings under Earthquakes in Barcelona, Spain. Computer-Aided Civ Infrastruct Eng 21:573–593. https://doi.org/10.1111/j.1467-8667.2006.00450.x

Battaglia L, Ferreira TM, Lourenço PB (2021) Seismic fragility assessment of masonry building aggregates: A case study in the old city Centre of Seixal, Portugal. Earthq Eng Struct Dyn 50:1358–1377. https://doi.org/10.1002/eqe.3405

Blasone V, Basaglia A, De Risi R et al (2022) A simplified model for seismic safety assessment of reinforced concrete buildings: framework and application to a 3-storey plan-irregular moment resisting frame. Eng Struct 250:113348. https://doi.org/10.1016/j.engstruct.2021.113348

Blasone V, Huseynli S, De Luca F et al (2025) Incorporating soil-structure interaction into simplified numerical models for fragility analysis of RC structures. Earthq Eng Struct Dyn 54:393–412. https://doi.org/10.1002/eqe.4259

Borzi B, Crowley H, Pinho R (2008) Simplified Pushover-Based Earthquake Loss Assessment (SP-BELA) Method for Masonry Buildings. Int J Architectural Herit 2:353–376. https://doi.org/10.1080/15583050701828178

Bozorgnia Y, Abrahamson NA, Ahdi SK et al (2022) NGA-Subduction research program. Earthq Spectra 38:783–798. https://doi.org/10.1177/87552930211056081

Bozorgnia Y, Abrahamson NA, Atik L, Al et al (2014) NGA-West2 Research Project. Earthq Spectra 30:973–987. https://doi.org/10.1193/072113EQS209M

Bull D (2013) Earthquakes and the effects on structures: Some of the lessons learnt. Australian J Struct Eng. https://doi.org/10.7158/S12-034.2013.14.2. 14:

Calvi GM, Pinho R, Crowley H (2006) State-of-the-knowledge on the period elongation of RC buildings during strong ground shaking. In: 1st European Conference on earthquake engineering and seismology, Geneva

Cornell CA, Jalayer F, Hamburger RO et al (2002) Steel moment frame guidelines. In: Federal Emergency Management Agency (FEMA) Guidelines, pp 526–533

Crowley H, Borzi B, Pinho R et al (2008) Comparison of Two Mechanics-Based Methods for Simplified Structural Analysis in Vulnerability Assessment. Adv Civil Eng 2008:1–19. https://doi.org/10.1155/2008/438379

Crowley H, Pinho R (2006) Simplified equations for estimating the period of vibration of existing buildings. In: 1st European conference on earthquake engineering and seismology, Geneva

Crowley H, Silva V, Martins L et al (2021) Open models and software for assessing the vulnerability of the European building stock. pp 2678–2688

Del Carpio RM, Mosqueda G, Lignos DG (2019) Experimental investigation of steel building gravity framing systems under strong earthquake shaking. Soil Dyn Earthq Eng 116:230–241. https://doi.org/10.1016/j.soildyn.2018.10.017

Di Pasquale G, Orsini G, Romeo RW (2005) New developments in seismic risk assessment in Italy. Bull Earthq Eng 3:101–128. https://doi.org/10.1007/s10518-005-0202-1

Dolce M, Kappos A, Masi A et al (2006) Vulnerability assessment and earthquake damage scenarios of the building stock of Potenza (Southern Italy) using Italian and Greek methodologies. Eng Struct 28:357–371. https://doi.org/10.1016/j.engstruct.2005.08.009

Dávalos H, Miranda E (2019) Evaluation of bias on the probability of collapse from amplitude scaling using spectral-shape-matched records. Earthq Eng Struct Dyn 48:970–986. https://doi.org/10.1002/eqe.3172

Eads L, Miranda E, Krawinkler H, Lignos DG (2013) An efficient method for estimating the collapse risk of structures in seismic regions. Earthq Eng Struct Dyn 42:25–41. https://doi.org/10.1002/eqe.2191
Eads L, Miranda E, Lignos DG (2015) Average spectral acceleration as an intensity measure for collapse risk assessment. Earthq Eng Struct Dyn 44:2057–2073. https://doi.org/10.1002/eqe.2575
Eladly MM (2017) Numerical study on masonry-infilled steel frames under vertical and cyclic horizontal loads. J Constr Steel Res 138:308–323. https://doi.org/10.1016/j.jcsr.2017.07.016
Elnashai A, Di Sarno L (2015) Fundamentals of earthquake engineering: from source to fragility, 2nd edn. Wiley
EN 1991-1-4 (2004) Eurocode 1: actions on structures—Part 1–4: general actions—Wind actions
Erkoseoglu G, Erberik MA, Citiloglu C (2014) A parametric study on unreinforced and confined masonry wall behavior. In: 2nd European Conference on Earthquake Engineering and Seismology (2ECEES), Istanbul
Farsangi EN, Noori M, Gardoni P et al (2021) Reliability-Based Analysis and Design of Structures and Infrastructure. CRC, Boca Raton
Fayaz J, Torres-Rodas P, Medalla M, Naeim F (2023) Assessment of ground motion amplitude scaling using interpretable Gaussian process regression: Application to steel moment frames. Earthq Eng Struct Dyn 52:2339–2359. https://doi.org/10.1002/eqe.3810
FEMA (2012a) Hazus®-MH 2.1 technical manual. Washington, DC
FEMA (2012b) Next-generation methodology for seismic performance assessment of buildings. Prepared by the Applied Technology Council for the Federal Emergency Management Agency, Report No. FEMA P-58. Washington, DC
FEMA (2024a) HAZUS 6.1 earthquake model technical manual. Washington, DC
FEMA (2024b) Hazus 6.1 Inventory technical manual. Washington, DC
Gaetani d'Aragona M, Polese M, Prota A (2020) Stick-IT: A simplified model for rapid estimation of IDR and PFA for existing low-rise symmetric infilled RC building typologies. Eng Struct 223:111182. https://doi.org/10.1016/j.engstruct.2020.111182
Gautam D, Chaulagain H (2016) Structural performance and associated lessons to be learned from world earthquakes in Nepal after 25 April 2015 (MW 7.8) Gorkha earthquake. Eng Fail Anal 68:222–243. https://doi.org/10.1016/j.engfailanal.2016.06.002
Gentile R, Galasso C (2021) Accounting for directivity-induced pulse-like ground motions in building portfolio loss assessment. Bull Earthq Eng 19:6303–6328. https://doi.org/10.1007/s10518-020-00950-9
Gentile R, Galasso C (2022) Surrogate probabilistic seismic demand modelling of inelastic single-degree-of-freedom systems for efficient earthquake risk applications. Earthq Eng Struct Dyn 51:492–511. https://doi.org/10.1002/eqe.3576
Günay S, Mosalam KM (2013) PEER Performance-Based Earthquake Engineering Methodology, Revisited. J Earthquake Eng 17:829–858. https://doi.org/10.1080/13632469.2013.787377
Goda K, Atkinson GM (2011) Seismic performance of wood-frame houses in south-western British Columbia. Earthq Eng Struct Dyn 40:903–924. https://doi.org/10.1002/eqe.1068
Gondaliya KM, Amin J, bhaiya V et al (2023) Seismic Vulnerability Assessment of Indian Code Compliant RC Frame Buildings. J Vib Eng Technol 11:207–231. https://doi.org/10.1007/s42417-022-00573-1
Goulet CA, Kishida T, Ancheta TD et al (2021) PEER NGA-East database. Earthq Spectra 37:1331–1353. https://doi.org/10.1177/87552930211015695
Haach VG, Vasconcelos G, Lourenço PB (2010) Experimental Analysis of Reinforced Concrete Block Masonry Walls Subjected to In-Plane Cyclic Loading. J Struct Eng 136:452–462. https://doi.org/10.1061/(ASCE)ST.1943-541X.0000125
Heresi P, Miranda E (2021) Intensity Measures for Regional Seismic Risk Assessment of Low-Rise Wood-Frame Residential Construction. J Struct Eng. https://doi.org/10.1061/(ASCE)ST.1943-541X.0002859. 147:
Jalayer F, Cornell CA (2009) Alternative non-linear demand estimation methods for probability-based seismic assessments. Earthq Eng Struct Dyn 38:951–972. https://doi.org/10.1002/eqe.876
Jalayer F, De Risi R, Manfredi G (2015) Bayesian Cloud Analysis: Efficient structural fragility assessment using linear regression. Bull Earthq Eng 13:1183–1203. https://doi.org/10.1007/s10518-014-9692-z
Jalayer F, Ebrahimian H, Miano A et al (2017) Analytical fragility assessment using unscaled ground motion records. Earthq Eng Struct Dyn 46:2639–2663. https://doi.org/10.1002/eqe.2922
Jamšek A, Dolšek M (2020) Seismic analysis of older and contemporary reinforced concrete frames with the improved fish-bone model. Eng Struct 212:110514. https://doi.org/10.1016/j.engstruct.2020.110514
Johnson K, Villani M, Bayliss K et al (2023) Global seismic hazard map
Jouneghani HG, Haghollahi A (2020) Assessing the seismic behavior of steel moment frames equipped by elliptical brace through incremental dynamic analysis (IDA). Earthq Eng Eng Vib 19:435–449. https://doi.org/10.1007/s11803-020-0572-z

Karanikoloudis G, Lourenço PB (2018) Structural assessment and seismic vulnerability of earthen historic structures. Application of sophisticated numerical and simple analytical models. Eng Struct 160:488–509. https://doi.org/10.1016/j.engstruct.2017.12.023

Karim Zadeh Z, Silva V, Yepes-Estrada C et al (2025) Development of a global earthquake impact database (GEID) for the verification and calibration of loss models. Earthq Spectra. https://doi.org/10.1002/esp4.70006

Lallemant D, Kiremidjian A, Burton H (2015) Statistical procedures for developing earthquake damage fragility curves. Earthq Eng Struct Dyn 44:1373–1389. https://doi.org/10.1002/eqe.2522

Lang DH, Kumar A, Sulaymanov S, Meslem A (2018) Building typology classification and earthquake vulnerability scale of Central and South Asian building stock. J Building Eng 15:261–277. https://doi.org/10.1016/j.jobe.2017.11.022

Loss C, Piazza M, Zonta D (2013) A New Method to Assess the Seismic Vulnerability of Existing Wood Frame Buildings. Adv Mat Res 778:486–494. https://doi.org/10.4028/www.scientific.net/AMR.778.486

Lotfy I, Mohammadalizadeh T, Ahmadi F, Soroushian S (2022) Fragility Functions for Displacement-based Seismic Design of Reinforced Masonry Wall Structures. J Earthquake Eng 26:33–51. https://doi.org/10.1080/13632469.2019.1659881

Lu X, Han B, Hori M et al (2014) A coarse-grained parallel approach for seismic damage simulations of urban areas based on refined models and GPU/CPU cooperative computing. Adv Eng Softw 70:90–103. https://doi.org/10.1016/j.advengsoft.2014.01.010

Lu X, Tian Y, Wang G, Huang D (2018) A numerical coupling scheme for nonlinear time history analysis of buildings on a regional scale considering site-city interaction effects. Earthq Eng Struct Dyn 47:2708–2725. https://doi.org/10.1002/eqe.3108

Luzi L, Lanzano G, Felicetta C et al (2020) Engineering strong motion database (ESM) (Version 2.0)

Magenes G, Calvi GM (1992) Cyclic behaviour of brick masonry walls. In: 10th World Conference on Earthquake Engineering (10WCEE). A.A. Balkema, Rotterdam

Markulak D, Radić I, Sigmund V (2013) Cyclic testing of single bay steel frames with various types of masonry infill. Eng Struct 51:267–277. https://doi.org/10.1016/j.engstruct.2013.01.026

Martins L, Silva V (2021) Development of a fragility and vulnerability model for global seismic risk analyses. Bull Earthq Eng 19:6719–6745. https://doi.org/10.1007/s10518-020-00885-1

Martins L, Silva V, Marques M et al (2016) Development and assessment of damage-to-loss models for moment-frame reinforced concrete buildings. Earthq Eng Struct Dyn 45:797–817. https://doi.org/10.1002/eqe.2687

McCormick J, DesRoches R, Fugazza D, Auricchio F (2007) Seismic Assessment of Concentrically Braced Steel Frames with Shape Memory Alloy Braces. J Struct Eng 133:862–870. https://doi.org/10.1061/(ASCE)0733-9445(2007)133:6(862)

McKenna F (2011) OpenSees: A framework for earthquake engineering simulation. Comput Sci Eng 13:58–66. https://doi.org/10.1109/MCSE.2011.66

Murcia-Delso J, Shing PB (2012) Fragility Analysis of Reinforced Masonry Shear Walls. Earthq Spectra 28:1523–1547. https://doi.org/10.1193/1.4000075

Nafeh AMB, Aljawhari K, Ettore A et al (2026a) OQ-VMTK: An open-source toolkit for earthquake vulnerability modelling applications. Earthq Spectra (under review)

Nafeh AMB, Aljawhari K, Silva V (2026b) A new global vulnerability model for regional seismic risk assessments: Part 2 – Non-structural and building content vulnerability. Bulletin of earthquake engineering (Under Review)

Nafeh AMB, O'Reilly GJ (2022) Unbiased simplified seismic fragility estimation of non-ductile infilled RC structures. Soil Dyn Earthq Eng 157:107253. https://doi.org/10.1016/j.soildyn.2022.107253

Nafeh AMB, O'Reilly GJ (2024) Fragility functions for non-ductile infilled reinforced concrete buildings using next-generation intensity measures based on analytical models and empirical data from past earthquakes. Bull Earthq Eng 22:4983–5021. https://doi.org/10.1007/s10518-024-01955-4

National Research Institute for Earth Science and Disaster Resilience (2019) NIED K-NET, KiK-net strong-motion seismograph networks.

Nettis A, Gentile R, Raffaele D et al (2021) Cloud Capacity Spectrum Method: Accounting for record-to-record variability in fragility analysis using nonlinear static procedures. Soil Dyn Earthq Eng 150:106829. https://doi.org/10.1016/j.soildyn.2021.106829

Nucera F, Santini A, Tripodi E, Caliò I (2012) Seismic vulnerability assessment of confined masonry buildings by macro-element modeling: a case study. In: 15th World Conference on Earthquake Engineering (15WCEE). Lisbon

O'Reilly GJ (2021) Limitations of Sa(T1) as an intensity measure when assessing non-ductile infilled RC frame structures. Bull Earthq Eng 19:2389–2417. https://doi.org/10.1007/s10518-021-01071-7

Parra PF, Arteta CA, Moehle JP (2019) Modeling criteria of older non-ductile concrete frame–wall buildings. Bull Earthq Eng 17:6591–6620. https://doi.org/10.1007/s10518-019-00697-y

Perez Gavilan JJ, Flores LE, Alcocer SM (2015) An Experimental Study of Confined Masonry Walls with Varying Aspect Ratios. Earthq Spectra 31:945–968. https://doi.org/10.1193/090712EQS284M
Porter K, Kennedy R, Bachman R (2007) Creating fragility functions for performance-based earthquake engineering. Earthq Spectra 23:471–489. https://doi.org/10.1193/1.2720892
Radnić J, Baloević G, Matešan D, Smilović M (2013) On a numerical model for static and dynamic analysis of in-plane masonry infilled steel frames. Materwiss Werksttech 44:423–430. https://doi.org/10.1002/mawe.201300146
Raghunandan M, Liel AB, Luco N (2015) Aftershock collapse vulnerability assessment of reinforced concrete frame structures. Earthq Eng Struct Dyn 44:419–439. https://doi.org/10.1002/eqe.2478
Ramirez CM, Lignos DG, Miranda E, Kolios D (2012) Fragility functions for pre-Northridge welded steel moment-resisting beam-to-column connections. Eng Struct 45:574–584. https://doi.org/10.1016/j.engstruct.2012.07.007
Ricci P, Verderame GM, Manfredi G (2011) Analytical investigation of elastic period of infilled RC MRF buildings. Eng Struct 33:308–319. https://doi.org/10.1016/j.engstruct.2010.10.009
Romão X, Pereira N, Castro JM et al (2021) European building vulnerability data repository
Sabelli R, Mahin S, Chang C (2003) Seismic demands on steel braced frame buildings with buckling-restrained braces. Eng Struct 25:655–666. https://doi.org/10.1016/S0141-0296(02)00175-X
Sen T (2009) Fundamentals of seismic loading on structures. Wiley
Shedid MT, Drysdale RG, El-Dakhakhni WW (2008) Behavior of Fully Grouted Reinforced Concrete Masonry Shear Walls Failing in Flexure: Experimental Results. J Struct Eng 134:1754–1767. https://doi.org/10.1061/(ASCE)0733-9445(2008)134:11(1754)
Silva V (2019) Uncertainty and Correlation in Seismic Vulnerability Functions of Building Classes. Earthq Spectra 35:1515–1539. https://doi.org/10.1193/013018EQS031M
Silva V, Amo-Oduro D, Calderon A et al (2020) Development of a global seismic risk model. Earthq Spectra 36:372–394. https://doi.org/10.1177/8755293019899953
Silva V, Brzev S, Scawthorn C et al (2022) A Building Classification System for Multi-hazard Risk Assessment. Int J Disaster Risk Sci 13:161–177. https://doi.org/10.1007/s13753-022-00400-x
Silveira D, Varum H, Costa A et al (2018) Seismic behavior of two Portuguese adobe buildings: Part I - in-plane cyclic testing of a full-scale adobe wall. Int J Architectural Herit 12:922–935. https://doi.org/10.1080/15583058.2017.1423131
So E (2016) Estimating fatality rates for earthquake loss models. Springer
Soleimani R, Khosravi H, Hamidi H (2019) Substitute Frame and adapted Fish-Bone model: Two simplified frames representative of RC moment resisting frames. Eng Struct 185:68–89. https://doi.org/10.1016/j.engstruct.2019.01.127
Stafford PJ (2008) Conditional Prediction of Absolute Durations. Bull Seismol Soc Am 98:1588–1594. https://doi.org/10.1785/0120070207
Suzuki A, Iervolino I (2020) Intensity measure conversion of fragility curves. Earthq Eng Struct Dyn 49:607–629. https://doi.org/10.1002/eqe.3256
Suzuki A, Iervolino I (2021) Seismic Fragility of Code-conforming Italian Buildings Based on SDoF Approximation. J Earthquake Eng 25:2873–2907. https://doi.org/10.1080/13632469.2019.1657989
Tarque N, Crowley H, Pinho R, Varum H (2012) Displacement-Based Fragility Curves for Seismic Assessment of Adobe Buildings in Cusco, Peru. Earthq Spectra 28:759–794. https://doi.org/10.1193/1.4000001
Tarquini D, de Almeida JP, Beyer K (2019) Experimental investigation on the deformation capacity of lap splices under cyclic loading. Bull Earthq Eng 17:6645–6670. https://doi.org/10.1007/s10518-019-00692-3
Tasnimi AA, Mohebkhah A (2011) Investigation on the behavior of brick-infilled steel frames with openings, experimental and analytical approaches. Eng Struct 33:968–980. https://doi.org/10.1016/j.engstruct.2010.12.018
Tischer H, Mitchell D, McClure G (2012) Ambient Vibration Measurements of Dynamic Properties of School Buildings in Montreal, Quebec. Structures Congress 2012. American Society of Civil Engineers, Reston, VA, pp 2279–2290
Ugalde D, Lopez-Garcia D (2020) Analysis of the seismic capacity of Chilean residential RC shear wall buildings. J Building Eng 31:101369. https://doi.org/10.1016/j.jobe.2020.101369
Ugalde D, Parra PF, Lopez-Garcia D (2019) Assessment of the seismic capacity of tall wall buildings using nonlinear finite element modeling. Bull Earthq Eng 17:6565–6589. https://doi.org/10.1007/s10518-019-00644-x
Vamvatsikos D, Cornell CA (2002) Incremental dynamic analysis. Earthq Eng Struct Dyn 31:491–514. https://doi.org/10.1002/eqe.141
Vijayanarayanan AR, Goswami R, Murty CVR (2017) Estimation of storey stiffness in multi-storey buildings. In: Proceedings of the 16th World Conference on Earthquake Engineering (16WCEE), Santiago, Chile, January 9–13, 2017

Villar-Vega M, Silva V, Crowley H et al (2017) Development of a Fragility Model for the Residential Building Stock in South America. Earthq Spectra 33:581–604. https://doi.org/10.1193/010716EQS005M
Voon KC, Ingham JM (2006) Experimental In-Plane Shear Strength Investigation of Reinforced Concrete Masonry Walls. J Struct Eng 132:400–408. https://doi.org/10.1061/(ASCE)0733-9445(2006)132:3(400)
Xiong C, Lu X, Guan H, Xu Z (2016) A nonlinear computational model for regional seismic simulation of tall buildings. Bull Earthq Eng 14:1047–1069. https://doi.org/10.1007/s10518-016-9880-0
Yepes-Estrada C, Calderon A, Costa C et al (2023) Global building exposure model for earthquake risk assessment. Earthq Spectra 39:2212–2235. https://doi.org/10.1177/87552930231194048
Zareian F, Medina RA (2010) A practical method for proper modeling of structural damping in inelastic plane structural systems. Comput Struct 88:45–53. https://doi.org/10.1016/j.compstruc.2009.08.001

**Publisher's note** Springer Nature remains neutral with regard to jurisdictional claims in published maps and institutional affiliations.